



Photocatalytic reduction elimination of UO_2^{2+} pollutant under visible light with metal-free sulfur doped $\text{g-C}_3\text{N}_4$ photocatalyst



Changhai Lu^a, Peng Zhang^c, Shujuan Jiang^{a,*}, Xi Wu^a, Shaoqing Song^{a,*}, Mingshan Zhu^c, Zaizhu Lou^c, Zhe Li^{b,*}, Fen Liu^a, Yunhai Liu^{a,*}, Yun Wang^a, Zhanggao Le^{a,*}

^a Key Laboratory for Radioactive Geology and Exploration Technology, Fundamental Science for National Defense, East China University of Technology, Nanchang 330013, PR China

^b Key Laboratory of Catalysis and Materials Science of the State Ethnic Affairs Commission & Ministry of Education, South-Central University for Nationalities, Wuhan, Hubei Province 430074, PR China

^c The Institute of Scientific and Industrial Research (SANKEN), Osaka University, Mihogaoka 8-1, Ibaraki, Osaka 567-0047, Japan

ARTICLE INFO

Article history:

Received 27 May 2016

Received in revised form 13 July 2016

Accepted 19 July 2016

Available online 20 July 2016

Keywords:

Photocatalysis

$\text{g-C}_3\text{N}_4$

Sulfur doping

Uranium reduction

Visible light

ABSTRACT

Reduction of soluble U(VI) to insoluble U(IV) oxide has been considered as an important approach to eliminate radioactive pollution and recycle uranium resource. The technology is hindered by the high cost, consumption of chemicals, and parallel generation of toxic wastes which are severe challenges today. In this paper, the photocatalytic reduction technology was utilized to eliminate UO_2^{2+} pollutant by constructing the highly efficient metal-free photocatalysts. Doping sulfur for substituting the lattice nitrogen of $\text{g-C}_3\text{N}_4$ ($\text{S-g-C}_3\text{N}_4$) modifies the electronic structure of $\text{g-C}_3\text{N}_4$ that displays the narrowed band-gap with the tuned conduction band and valence band levels as well as a good ability of electron-hole separation and carrier mobility. The photoreactivity of UO_2^{2+} reduction for $\text{S-g-C}_3\text{N}_4$ is 1.86 and 32 times of that for pristine $\text{g-C}_3\text{N}_4$ and N-TiO_2 under visible light irradiation. The substitution of sulfur for lattice nitrogen was experimentally and theoretically identified as the cause of this unique electronic structure and, consequently, the excellent photoreactivity of $\text{S-g-C}_3\text{N}_4$ in the reduction of UO_2^{2+} . The results may shed light on improving the reduction technology to eliminate U(VI) pollutant by doping strategies to design potentially efficient photocatalysts.

© 2016 Elsevier B.V. All rights reserved.

1. Introduction

With the rapid development of nuclear industry, much attention has been given to the harm of nuclear waste released from uranium mining, milling, and processing [1,2]. Study has confirmed that a long-term exposure to uranium would cause serious health problems (e.g., severe liver damage, kidney damage and eventually death) [3]. Therefore, how to eliminate uranium pollution is an important issue in the protection of environment and alleviation of the nuclear material resource [4,5]. It is seen that uranium species exist in several chemical states (e.g., U(0), U(III), U(IV), and U(VI)), in which the predominant chemical states in the ambient environment are soluble U(VI) and slightly soluble U(IV) [6–9]. Therefore, reduction of soluble U(VI) to insoluble U(IV) oxide has been proposed as an important approach to eliminate radioactive pollution and reuse uranium resource [8,10–13]. However, most of reported

reduction strategies are expensive and involve a high consumption of chemicals, generating parallel toxic wastes [14]. Semiconductor photocatalysis, a green strategy that can reductively remove harmful heavy metals using semiconductor photocatalysts under sun light irradiation, provides a new option to address the above challenges [15–20]. For example, TiO_2 particles were employed as photocatalysts for photo-induced reduction of U(VI) under UV with the aid of humic acid, formic acid, and 2-propanol [14,17–19]. TiO_2 is undoubtedly the most studied semiconductor photocatalyst with its low cost, high activity and stability. However, due to its wide band gap (3.2 eV), TiO_2 cannot be activated by the visible light. In order to make full use of solar energy for photocatalytically reducing U(VI) to U(IV), it is desirable to develop efficient visible light-responsive metal/metal oxides semiconductor photocatalysts or even metal-free photocatalysts.

Recently, graphitic carbon nitride ($\text{g-C}_3\text{N}_4$) has attracted intensive interest for its promising applications in photo-splitting water, photo-decomposition of organic pollutants, and photosynthesis under visible light, because this material shows good visible light response (up to 455 nm), high thermal, and chemical stability

* Corresponding authors.

E-mail address: sqsong@ecit.edu.cn (S. Song).

[21–40]. Study has revealed that the conduction band position of pristine g-C₃N₄ is at around –1.23 V (vs. SHE at pH 7) [26], which is more negative than the reduction potential of UO₂²⁺/U⁴⁺ (0.267 V), UO₂²⁺/UO₂ (0.411 V), and U₄O₉/UO₂ (0.456 V). Accordingly, it will be very meaningful to investigate photocatalytic reduction of UO₂²⁺ with metal-free g-C₃N₄ as photocatalyst. However, the photocatalytic activity of the g-C₃N₄ is usually restricted by low efficiency due to the insufficient sunlight absorption and the fast recombination of photo-induced electron-hole pairs. It is known that, doping, especially anion doping, is an effective strategy to modulate absorbance, redox potentials, and mobility of photo-induced charge carriers [41–52]. However, some key issues such as the origin of non-metal doping-induced visible light absorption, the nature of the chemical states created, and the locations of the dopants are not yet well understood. Based on first-principle calculations for elements doping [53], we consider that two rules should be followed for anion dopant: one is that the electronegativity of the anion dopant must be lower than that of the substituted lattice atom; the other is that dopant anion should have a radius comparable to that of the substituted lattice atom. In this work, to demonstrate the above considerations, sulfur, which has a smaller electronegativity and larger radius than nitrogen (2.58 vs 3.04, 1.09 vs 0.75 Å), was chosen as dopant into g-C₃N₄ for the photocatalytic reduction of U(VI). The desirable electronic structural properties of the sulfur-doped g-C₃N₄ were revealed by spectroscopy characterizations. The remarkable electronic structure exhibits potency in achieving high photo-reduction activity for the reduction of U(VI). The origin of the unique electronic structure and, consequently, the excellent photo-reduction performance of the S-g-C₃N₄ are explored both experimentally and theoretically, suggesting doping strategies to design potentially efficient photocatalysts for photocatalytic reduction elimination of U(VI) pollutants.

2. Experimental

2.1. Photocatalyst preparation

All of the chemical reagents were of analytic grade without further purification. In detail, 10 g of urea or thiourea powder were heated to 520 °C in air at a heating rate of 2.5 °C/min. The temperature was kept at 520 °C for 2 h and then cooled to room temperature. The as-prepared samples prepared with urea or thiourea were labeled as g-C₃N₄ or S₁-g-C₃N₄, respectively. It is reported that the sulfur doping into g-C₃N₄ with a tuned content is not an easy process and sublimed sulfur can mediate polymerization of the g-C₃N₄ [29], and therefore CS₂ was further selected as sulfur source and sublimed sulfur was used to improve the doping of sulfur from CS₂ precursor into g-C₃N₄ or S₁-g-C₃N₄. 0.005 g sulfur powder was dissolved into 8 ml of CS₂, and then 25 ml aqueous solution including 10 g of urea or thiourea was added into the sulfur solution and ultrasonicated for 25 min, and the mixture was agitated at 40 °C for 0.5 h. Afterwards, the obtained solids were heated to 520 °C at a heating rate of 2.5 °C/min and kept at the temperature for 2 h. The obtained samples were denoted as S₂-g-C₃N₄ and S₃-g-C₃N₄ corresponding to urea and thiourea as precursors.

2.2. Characterization

The X-ray diffraction (XRD) patterns of the samples were performed on a D/Max-RB X-ray diffractometer (Rigaku) using Cu K α radiation at a scanning rate (2 θ) of 0.05° s⁻¹. The morphology was observed by transmission electron microscope (TEM, JEOL-JEM-1005 at 100 kV), and high resolution TEM (HRTEM, JEM2010 at 200 kV). X-ray photoelectron spectroscopy (XPS) measurements were performed on an ESCALAB250xi spectrometer (Thermon

Scientific). The binding energy (BE) was referenced to the C 1s peak at 284.8 eV of the surface adventitious carbon. Micromeritics ASAP2020 nitrogen adsorption apparatus (USA) was used to record Brunauer–Emmett–Teller (BET) specific surface area of photocatalysts and all of the samples were degassed at 180 °C before analysis. The pore size distributions were evaluated using desorption data with Barret–Joyner–Halender (BJH) method. The BET surface area was determined by a multipoint BET method to analyze the adsorption data in the relative pressure (P/P₀) range from 0.05 to 0.25. UV-vis diffuse reflection spectra (DRS) were obtained by using a dry-pressed disk sample with a UV-vis spectrophotometer (UV-2550, Shimadzu, Japan), and BaSO₄ is used as reflectance standard. Photoluminescence (PL) spectra were obtained on a Fluorescence Spectrophotometer (F-7000, Hitachi, Japan) at room temperature. The Photo Multiplier Tube voltage was 700 V, the scanning speed was 1200 nm/min, and the excitation wave-length was 380 nm. The widths used for the excitation and emission slit were both 1.0 nm. Photocurrent measurements were performed using an electrochemical analyzer (CHI 660D electrochemical workstation, Chenhua Instrument, Shanghai, China) in a conventional three-electrode configuration with working electrode, counter electrode, and reference electrode. The working electrodes prepared with samples have an active area of 0.5 cm², and a Pt wire and Ag/AgCl (saturating KCl) were used as the counter electrode and reference electrode, respectively. A 300 W Xe arc lamp equipped with an ultraviolet cutoff filter ($\lambda > 400$ nm) was utilized as the visible light source. The integrated visible light intensity measured with a visible light radiometer was 25 mW/cm², and Na₂SO₄ aqueous solution (1 M) was used as the electrolyte.

2.3. Photocatalytic tests

The as-prepared g-C₃N₄ samples were used as photocatalysts for the photocatalytic reduction of UO₂²⁺ solutions under the visible light irradiation. In the catalytic process, 0.10 g of the g-C₃N₄ samples was added into 200 ml of 0.12 mM UO₂²⁺ solution which was prepared by dissolving uranyl nitrate (UO₂(NO₃)₂·6H₂O) into mixture of deionized water and methanol (5 ml). A 350 W Xe lamp with a 420 nm cutoff filter was used as the visible light source. Before irradiation, the reduction reaction system was bubbled with nitrogen for 60 min to remove oxygen, which ensures that the reaction system was under anaerobic condition. And then, the mixed solution was magnetically stirred in the dark for 2 h to ensure the adsorption-desorption equilibrium. After illumination for a certain time, the absorbance of UO₂²⁺ was analyzed by UVmini-1240 using Arsenazo III Spectrophotometric method at wavelength of 650 nm. The absorbance intensity at different illumination time was transformed to the reduction ratio of UO₂²⁺, which is calculated with the following expression:

Reduction ratio of UO₂²⁺: $C/C_0 = (A_0 - A_t)/A_0 \times 100\%$, where A_0 and A_t are the absorbance intensities at 0 (after the dark adsorption) and t min, respectively. UO₂²⁺ solution without photocatalysts was also irradiated under visible light for 40 min.

2.4. Computational details

Density functional theory (DFT) calculations were performed using Perdew–Burke–Ernzerhof functionals with the combined basis sets of 3-21G* (C, H, N and S) and LanL2DZ (U). The atomic structures of the pristine and the sulfur-doped g-C₃N₄ were modeled by a truncated unit with three melems, in which two possible cases of nitrogen substituted by sulfur were considered. The peripheral C/N atoms were saturated with hydrogen atoms in order to avoid the boundary effect. U(VI) ion was encapsulated into the center of the g-C₃N₄ and S-g-C₃N₄ to investigate the binding

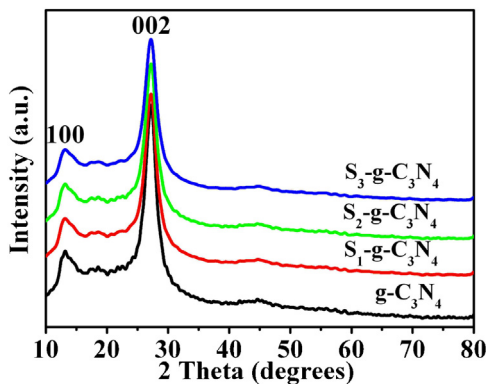


Fig. 1. XRD patterns for $\text{g-C}_3\text{N}_4$, $\text{S}_1\text{-g-C}_3\text{N}_4$, $\text{S}_2\text{-g-C}_3\text{N}_4$ and $\text{S}_3\text{-g-C}_3\text{N}_4$.

interactions of the complexes. BE of U(VI) and C_3N_4 catalyst was calculated as equation: $\text{BE} = \text{E}_{\text{U(VI)/cat}} - \text{E}_{\text{U(VI)}} - \text{E}_{\text{cat}}$.

3. Results and discussion

3.1. Composition and morphology of the photocatalysts

The crystalline structure of $\text{g-C}_3\text{N}_4$ is well preserved in the S doped $\text{g-C}_3\text{N}_4$ samples, as confirmed by two feature signals on the XRD pattern (Fig. 1). It is seen that two characteristic peaks were observed, and no obvious different pattern was displayed between $\text{g-C}_3\text{N}_4$ and $\text{S-g-C}_3\text{N}_4$ samples. The strong peak at 27.4° represents the inter-layer stacking of conjugated aromatic systems, which is indexed for graphitic materials as the (002) peak. A minor diffraction peak was located at 13.1° , which was indexed to the (100) plane corresponding to the in-plane structural packing of aromatic systems [27,39]. Notably, the XRD patterns for $\text{S-g-C}_3\text{N}_4$ samples showed the overall weakened diffraction peak intensity in comparison with $\text{g-C}_3\text{N}_4$, which can be attributed to the incomplete polymerization caused by sulfur doping. And the morphology and microstructure of $\text{g-C}_3\text{N}_4$ and $\text{S-g-C}_3\text{N}_4$ samples were investigated with TEM and HRTEM. In Fig. 2, $\text{g-C}_3\text{N}_4$ and $\text{S-g-C}_3\text{N}_4$ samples appear the nanosheet images, and the nanosheets contain many irregular pores with the diameters ranging from 5 nm to 40 nm. Compared with the $\text{g-C}_3\text{N}_4$, the $\text{S-g-C}_3\text{N}_4$ samples show more pores with small diameter size. Especially, $\text{S}_2\text{-g-C}_3\text{N}_4$ and $\text{S}_3\text{-g-C}_3\text{N}_4$ prepared by adding S and CS_2 into the solution of urea or thiourea present more pores with the diameter size of 5–12 nm, which would lower the degree of crystallization. Element mapping and EDS of FESEM indicates the existence and homogeneous distribution of S in the $\text{S-g-C}_3\text{N}_4$ (Fig. S1 in Supplementary material). Moreover, the nitrogen adsorption isotherms of $\text{S-g-C}_3\text{N}_4$ samples were similar and of type IV with H3 hysteresis loops, indicating the existence of slit-like pores resulted from the aggregates of plate-like particles (Fig. S2 in the Supplementary material). Furthermore, surface areas of the $\text{g-C}_3\text{N}_4$ and $\text{S-g-C}_3\text{N}_4$ samples revealed by BET method are calculated to be 8.2, 5.3, 15.5, and $12.7 \text{ m}^2/\text{g}$ for the $\text{g-C}_3\text{N}_4$, $\text{S}_1\text{-g-C}_3\text{N}_4$, $\text{S}_2\text{-g-C}_3\text{N}_4$, and $\text{S}_3\text{-g-C}_3\text{N}_4$, respectively.

The compositions and chemical states of $\text{g-C}_3\text{N}_4$ and the doped samples were further investigated by XPS. As shown in Fig. 3A, all the survey spectra are mainly comprised of C, N and O signals, in which the intensity of N signal is strongest due to the highest atomic ratio of N in $\text{g-C}_3\text{N}_4$ samples. The S signal cannot be detected in the survey spectra of three $\text{S-g-C}_3\text{N}_4$ samples because of its low doping content. In detail, no obvious BE shift of C 1s and N 1s core electrons suggests that the chemical states of the both carbon and nitrogen in the $\text{S-g-C}_3\text{N}_4$ samples are similar with those in the pristine $\text{g-C}_3\text{N}_4$ (Fig. 3B, C). In Fig. 3B, each C1s spectrum is mainly comprised of the standard reference carbon and the sp^2 bonded C in $\text{N}=\text{C}-\text{N}_2$ peaked

at 284.8 and 288.0 eV, respectively [35]. And the N 1s spectrum for each sample can be mainly deconvoluted into three components in Fig. 3C, which are characteristic of $\text{C}=\text{N}-\text{C}$ (398.8 eV), tertiary nitrogen C_3-N (399.6 eV), and $\text{C}-\text{N}-\text{H}$ (401.4 eV) [49]. The weakest peak was at 404.3 eV, which was assigned to the π -excitations [54]. In Fig. 3D of fine spectrum for S, one weak broad signal was detected for each $\text{S-g-C}_3\text{N}_4$ and this S 2p spectrum can be fitted into two components, i.e., the dominant peak at 163.9 eV from the C–S bond formed in $\text{S-g-C}_3\text{N}_4$ by substituting sulfur for lattice nitrogen,³⁴ and the weak peak at 166.1 eV from $\text{C}-\text{SO}_x-\text{C}$ bond [55]. Moreover, the intensity of the peak increased at 163.9 eV with increasing the sulfur content through tuning the precursor from thiourea to S/CS_2 /urea and S/CS_2 /thiourea. Simultaneously, the content of the C–S increased progressively from 0.08% to 0.34% and 0.49% corresponding to $\text{S}_1\text{-g-C}_3\text{N}_4$, $\text{S}_2\text{-g-C}_3\text{N}_4$, and $\text{S}_3\text{-g-C}_3\text{N}_4$. These results indicate that a continuous modulation on the content of sulfur doped into $\text{S-g-C}_3\text{N}_4$ samples has been achieved, which provides a good platform for investigating the doping effect of sulfur in $\text{S-g-C}_3\text{N}_4$ on the electronic structure and the performance in the photocatalytic reduction removal of UO_2^{2+} .

3.2. Optical absorption properties of photocatalysts

The change in the electronic band structure of $\text{g-C}_3\text{N}_4$ caused by the introduction of sulfur atom was investigated by UV-vis absorption spectroscopy. As shown in Fig. 4A, an additional absorption band ranging from 450 to 600 nm is formed in the UV-vis absorption spectra of $\text{S-g-C}_3\text{N}_4$ samples compared to the $\text{g-C}_3\text{N}_4$ because of the optical transition of the sulfur impurity within the gap [56,57]. Further analysis using the transformed Kubelka-Munk function versus the energy of the absorbed light shows that the intrinsic band gap decreases from 2.70 to 2.54, 2.49, and 2.38 eV corresponding to $\text{g-C}_3\text{N}_4$, $\text{S}_1\text{-g-C}_3\text{N}_4$, $\text{S}_2\text{-g-C}_3\text{N}_4$, and $\text{S}_3\text{-g-C}_3\text{N}_4$, respectively (Fig. 4B). In Fig. 4C of electrochemical Mott-Schottky, the positive slopes of the plots suggest that $\text{g-C}_3\text{N}_4$ and $\text{S-g-C}_3\text{N}_4$ samples are n-type semiconductors. From the intercept on the abscissa, the conduction band (CB) potential was obtained at approximately -1.44 , -1.45 , -1.48 , and -1.50 V (vs Ag/AgCl), i.e., -1.22 , -1.23 , -1.26 , -1.28 V (vs SHE) at pH=7 for $\text{g-C}_3\text{N}_4$, $\text{S}_1\text{-g-C}_3\text{N}_4$, $\text{S}_2\text{-g-C}_3\text{N}_4$, and $\text{S}_3\text{-g-C}_3\text{N}_4$, respectively. These data, combined with the band gap energies, allow us to calculate the valence band (VB) edges of samples at 1.48, 1.31, 1.23, and 1.10 V (vs SHE), corresponding to $\text{g-C}_3\text{N}_4$, $\text{S}_1\text{-g-C}_3\text{N}_4$, $\text{S}_2\text{-g-C}_3\text{N}_4$, and $\text{S}_3\text{-g-C}_3\text{N}_4$, as illustrated in Fig. 4D. Therefore, the obtained CB edges of the as-doped $\text{S-g-C}_3\text{N}_4$ samples are more negative than the reduction potential of $\text{UO}_2^{2+}/\text{U}^{4+}$ (0.267 V vs SHE, pH=7) and $\text{UO}_2^{2+}/\text{UO}_2$ (0.411 V vs SHE, pH=7), which can be satisfied with thermodynamic requirements. Furthermore, the high absorption in the range of 450–600 nm, as well as the narrowed band gap, indicated that sulfur doping provides the possibility, as expected, to improve the photoactivity of the $\text{g-C}_3\text{N}_4$ based photocatalysts in the photocatalytic reduction of UO_2^{2+} .

3.3. Photocatalytic activity and stability under visible light

According to the calculation with visual MINTEQA using the standard thermodynamic database, $(\text{UO}_2)_3(\text{OH})_5^+$ and $(\text{UO}_2)_4(\text{OH})_7^+$, are the main uranium species [58–60], and the surfaces of $\text{g-C}_3\text{N}_4$ samples are negatively charged at pH=7 by the Zeta potential tests (Fig. 5). Thus, the pH of the reduction reaction system was adjusted to 7.0 with the diluted NaOH solution. The photocatalytic performances of $\text{S-g-C}_3\text{N}_4$ photocatalysts, together with the pristine $\text{g-C}_3\text{N}_4$ for comparison, were evaluated in the photocatalytic reduction of UO_2^{2+} (Fig. 6A). In the dark adsorption experiments, the UO_2^{2+} ion concentration in the presence of photocatalysts firstly decreased and then kept constant after 120 min,

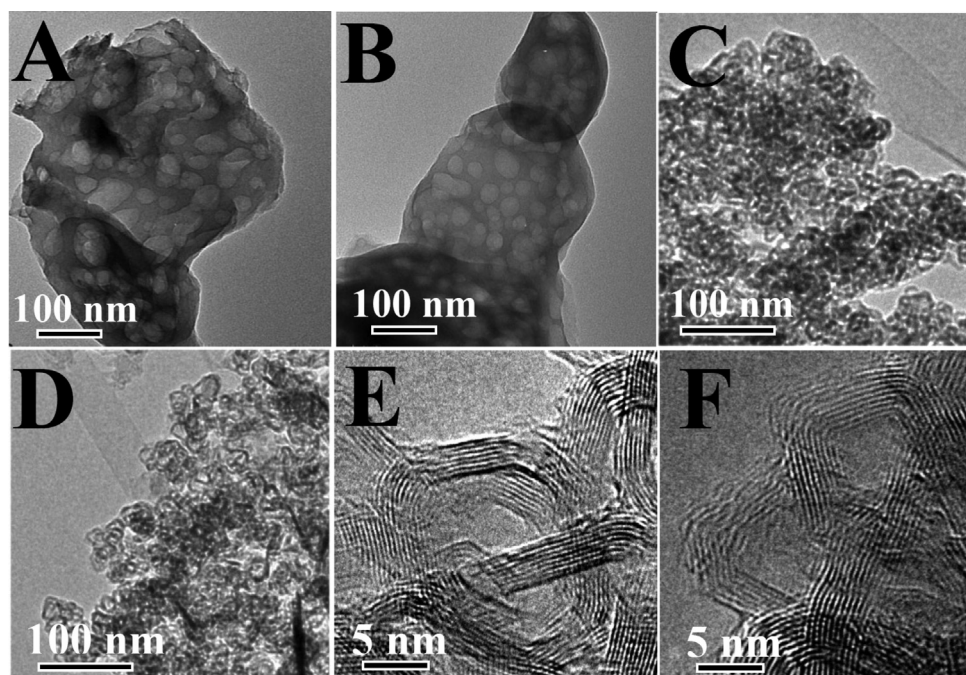


Fig. 2. TEM and HRTEM images for $\text{g-C}_3\text{N}_4$ (A), $\text{S}_1\text{-g-C}_3\text{N}_4$ (B), $\text{S}_2\text{-g-C}_3\text{N}_4$ (C, E) and $\text{S}_3\text{-g-C}_3\text{N}_4$ (D, F).

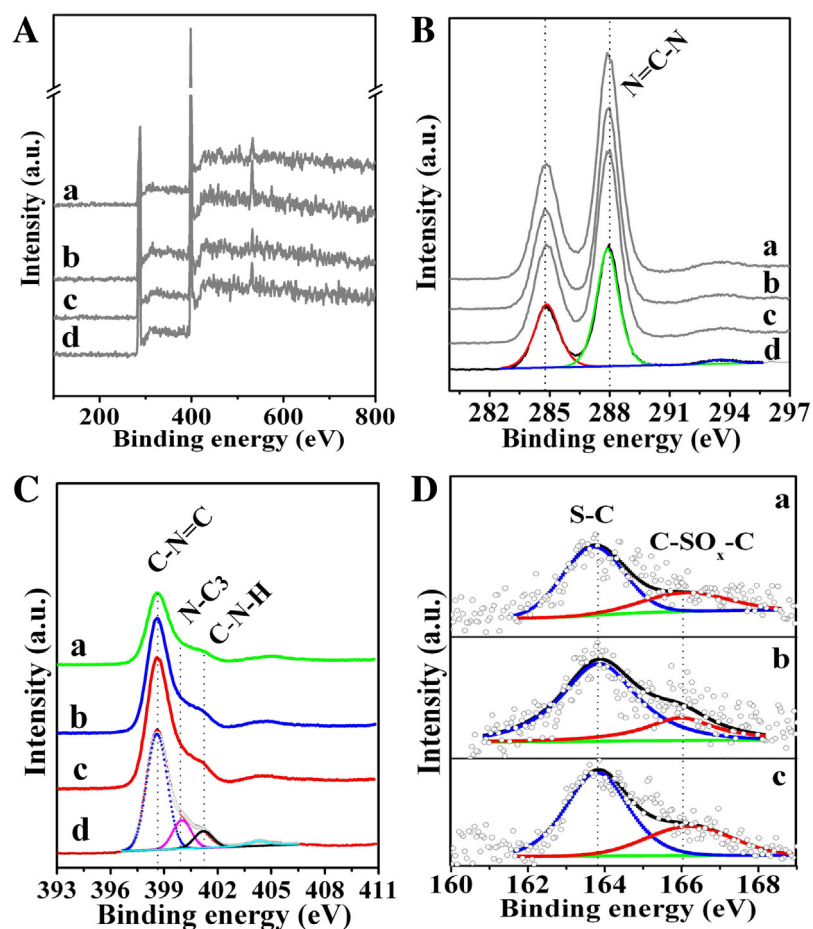


Fig. 3. XPS profiles for the $\text{g-C}_3\text{N}_4$ and S-doped $\text{g-C}_3\text{N}_4$. Survey spectra (A), high-resolution XPS spectra of C 1s (B), N 1s (C), and S 2p (D). The corresponding sample is (a) $\text{S}_1\text{-g-C}_3\text{N}_4$, (b) $\text{S}_2\text{-g-C}_3\text{N}_4$, (c) $\text{S}_3\text{-g-C}_3\text{N}_4$ and (d) $\text{g-C}_3\text{N}_4$.

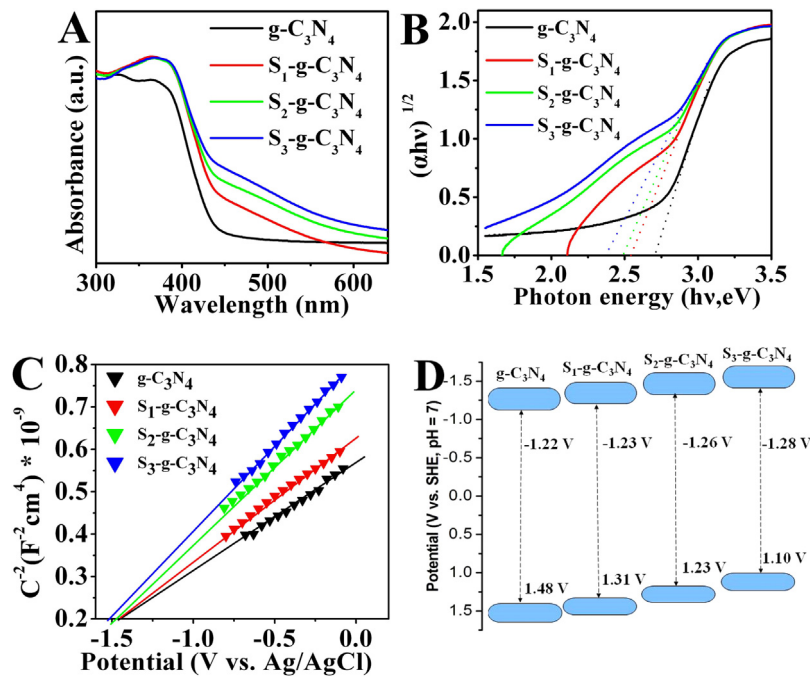


Fig. 4. (A) Optical absorption spectra of $\text{g-C}_3\text{N}_4$ and $\text{S}-\text{g-C}_3\text{N}_4$ samples; (B) plots of $(\alpha h\nu)^{1/2}$ vs. photon energy ($h\nu$); (C) electrochemical Mott-Schottky plots of $\text{g-C}_3\text{N}_4$ and $\text{S}-\text{g-C}_3\text{N}_4$ samples and (D) schematic of the electronic structure of $\text{g-C}_3\text{N}_4$ and $\text{S}-\text{g-C}_3\text{N}_4$ samples.

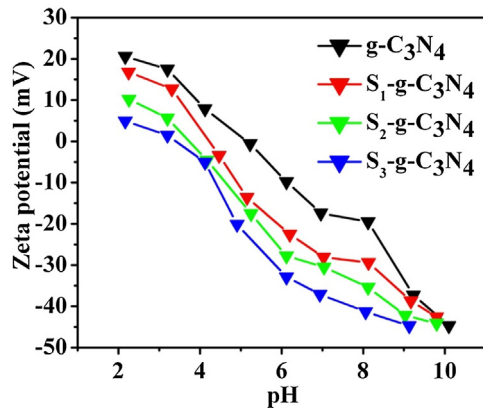


Fig. 5. Zeta potential tests for $\text{g-C}_3\text{N}_4$ and $\text{S}-\text{g-C}_3\text{N}_4$ samples at $\text{pH}=7$.

suggesting that the adsorption-desorption equilibrium between photocatalysts and UO_2^{2+} ion was achieved. UO_2^{2+} solution without photocatalysts was irradiated under visible light for 40 min, and the concentration showed no obvious decrease, indicating that

aqueous UO_2^{2+} ion is stable and the self-photolysis process can be ignored. Furthermore, the reduction of UO_2^{2+} proceeded rapidly in the presence of $\text{g-C}_3\text{N}_4$ and $\text{S}-\text{g-C}_3\text{N}_4$ photocatalysts under visible light irradiation. Nevertheless, the photocatalytic activities of $\text{g-C}_3\text{N}_4$ and $\text{S}-\text{g-C}_3\text{N}_4$ samples differed greatly, and followed the order of $\text{S}_3-\text{g-C}_3\text{N}_4 > \text{S}_2-\text{g-C}_3\text{N}_4 > \text{S}_1-\text{g-C}_3\text{N}_4 > \text{g-C}_3\text{N}_4$. For instance, under visible light irradiation for 20 min, the photocatalytic reduction ratios of UO_2^{2+} over $\text{S}_3-\text{g-C}_3\text{N}_4$, $\text{S}_2-\text{g-C}_3\text{N}_4$, $\text{S}_1-\text{g-C}_3\text{N}_4$, and $\text{g-C}_3\text{N}_4$ were 95%, 84%, 80%, and 71%, respectively. Moreover, the photocatalytic reaction rate constant (k) in the presence of $\text{S}_3-\text{g-C}_3\text{N}_4$, $\text{S}_2-\text{g-C}_3\text{N}_4$, $\text{S}_1-\text{g-C}_3\text{N}_4$, and $\text{g-C}_3\text{N}_4$ corresponds to 0.13, 0.10, 0.09, 0.07 min^{-1} , obtained using the pseudo-first-order model as expressed by [13,18]

$$\ln(C/C_0) = kt$$

Particularly, the k for the optimized $\text{S}_3-\text{g-C}_3\text{N}_4$ sample is 0.13 min^{-1} , which is 1.86 times of that for $\text{g-C}_3\text{N}_4$ (0.07 min^{-1}) (Fig. 6B). The chemical state of U on the surface of $\text{S}-\text{g-C}_3\text{N}_4$ was characterized by XPS (Fig. 7). The XPS spectrum of U 4f locates at the regions of 377–387 eV and 388–398 eV which correspond to the U 4f_{7/2} and its satellite peak. The U 4f_{7/2} signal can be deconvoluted

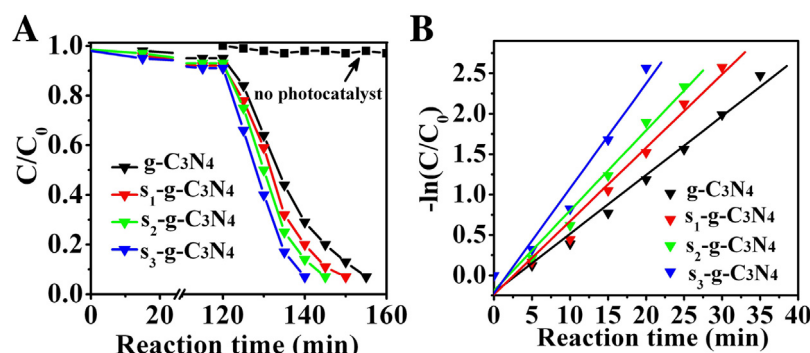


Fig. 6. (A) The variation of UO_2^{2+} concentration vs. illumination time with $\text{g-C}_3\text{N}_4$ and $\text{S}-\text{g-C}_3\text{N}_4$ as photocatalysts; and (B) the rate constant (k) of UO_2^{2+} reduction with $\text{g-C}_3\text{N}_4$ and $\text{S}-\text{g-C}_3\text{N}_4$ as photocatalysts.

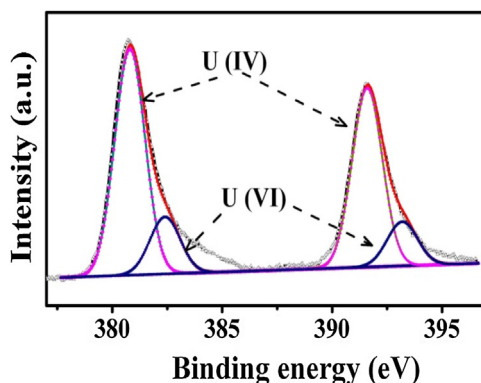


Fig. 7. XPS spectra of U 4f for the U element on the surface of $S_3\text{-}g\text{-}C_3\text{N}_4$.

into two components centered at 382.0 and 380.8 eV, ascribable to the characteristic signal of U^{6+} and U^{4+} species, respectively [12]. Thus, the results indicate that sulfur doping can promote the photocatalytic activities of $\text{g}\text{-}\text{C}_3\text{N}_4$ photocatalysts for the photocatalytic reduction of $\text{U}(\text{VI})$ to $\text{U}(\text{IV})$.

Moreover, the photocatalytic activity of $S\text{-}\text{g}\text{-}\text{C}_3\text{N}_4$ was further evaluated by comparing with the traditional photocatalytic reduction catalysts (e.g., SnIn_4S_8 , CdS -graphene, SnS_2 , and N-TiO_2) [61–64], and it is seen that the photocatalytic performances follow the order: $S_3\text{-}g\text{-}C_3\text{N}_4 > \text{SnIn}_4\text{S}_8 > \text{CdS}\text{-graphene} > \text{SnS}_2 > \text{N-TiO}_2$ (Fig. 8A). And the k of $S_3\text{-}g\text{-}C_3\text{N}_4$ is 2.65, 5.2, 6.8, and 32.5 times of that for SnIn_4S_8 (0.049 min^{-1}), $\text{CdS}\text{-graphene}$ (0.025 min^{-1}), SnS_2 (0.019 min^{-1}), and N-TiO_2 (0.004 min^{-1}), respectively (Fig. 8B). It is seen that the photocatalytic performance of metal-free $S\text{-}\text{g}\text{-}\text{C}_3\text{N}_4$ photocatalyst is even higher than the case of the metal-based ones, indicating $S\text{-}\text{g}\text{-}\text{C}_3\text{N}_4$ with a lower cost but higher performance has a great potential application in photocatalytic reduction of UO_2^{2+} .

Along with the photocatalytic activity for the reduction of UO_2^{2+} , the $S_3\text{-}g\text{-}C_3\text{N}_4$ presents excellent stability, as shown in Fig. 9. After each reaction, the photocatalysts were collected and separated by centrifugation from the suspension aqueous and reacted with the 1 mol/L HNO_3 solution to remove the $\text{U}(\text{IV})$ deposited on the surface of $S_3\text{-}g\text{-}C_3\text{N}_4$, and then washed by the deionized water. Afterward, the photocatalysts were dried in vacuum at 60°C for 2 h for the next recycle photocatalytic reduction reaction. FT-IR test was conducted to ensure the structure integrity of the recycled $S\text{-}\text{g}\text{-}\text{C}_3\text{N}_4$ (Fig. S3 in Supplementary material). The UO_2^{2+} removal efficiency of the five cycles is 0.13, 0.126, 0.125, 0.122, and 0.121 min^{-1} , meaning no obvious decline occurs in the photocatalytic activity of $S_3\text{-}g\text{-}\text{C}_3\text{N}_4$ in the reduction of UO_2^{2+} after five recycles. The preceding experimental results indicate that sulfur doping can turn $\text{g}\text{-}\text{C}_3\text{N}_4$

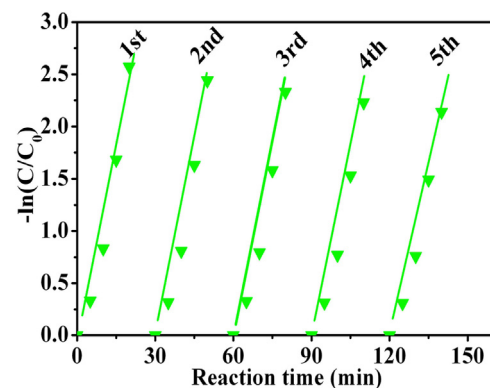


Fig. 9. Cycling runs of $S_3\text{-}g\text{-}C_3\text{N}_4$ for the photocatalytic reduction of UO_2^{2+} .

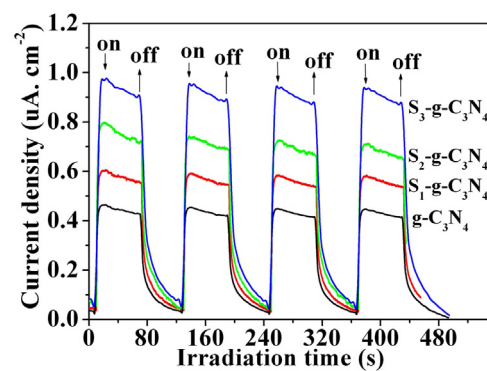


Fig. 10. Transient photocurrent responses of $\text{g}\text{-}\text{C}_3\text{N}_4$ and $S\text{-}\text{g}\text{-}\text{C}_3\text{N}_4$ samples in 1 M Na_2SO_4 aqueous solution under UV-vis light irradiation at 0.5 V vs Ag/AgCl .

into efficient metal-free photocatalyst for the reduction removal of $\text{U}(\text{VI})$ with high activity and excellent stability.

Furthermore, the essence of the high activity and excellent stability of $S\text{-}\text{g}\text{-}\text{C}_3\text{N}_4$ in the photocatalytic reduction of UO_2^{2+} was experimentally investigated by the transient photocurrent responses, because high photocurrent value represents more efficient separation of electrons and holes. As seen in Fig. 10, the images show the $i\text{-}t$ curves of the $\text{g}\text{-}\text{C}_3\text{N}_4$ and $S\text{-}\text{g}\text{-}\text{C}_3\text{N}_4$ samples with on-off cycles of intermittent irradiation at a bias potential of 0.5 V, and the photocurrent figures of the $\text{g}\text{-}\text{C}_3\text{N}_4$ and $S\text{-}\text{g}\text{-}\text{C}_3\text{N}_4$ are almost the same. When the light irradiated samples, the photocurrent value rapidly boosted, and meanwhile the values decreased to zero as the light turned off, indicating most of the photogenerated electrons ran across samples and transferred at the back contact to form photocurrent. Moreover, $S\text{-}\text{g}\text{-}\text{C}_3\text{N}_4$ samples show higher photo-

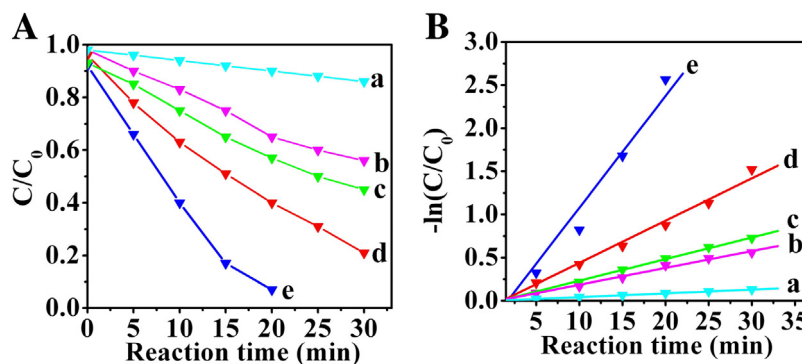


Fig. 8. (A) The variation of UO_2^{2+} concentration vs. illumination time; (B) the rate constant (k) of UO_2^{2+} reduction. (a) N-TiO_2 , (b) SnS_2 , (c) $\text{CdS}\text{-rGO}$, (d) SnIn_4S_8 , and (e) $S_3\text{-}g\text{-}C_3\text{N}_4$.

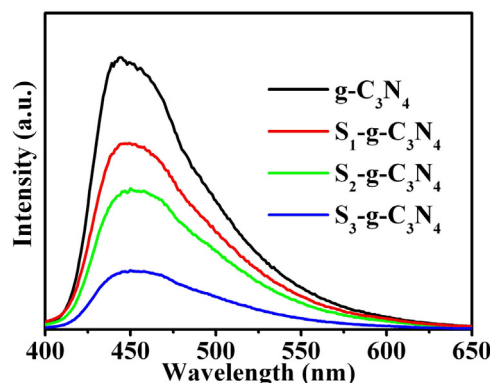


Fig. 11. PL spectra of $\text{g-C}_3\text{N}_4$ and $\text{S}-\text{g-C}_3\text{N}_4$ samples.

tocurrent intensity than $\text{g-C}_3\text{N}_4$, which illustrates that $\text{S}-\text{g-C}_3\text{N}_4$ has higher efficiency of electron-hole separation and lower rate of charge carrier recombination [65]. Moreover, the efficiency of the charge carrier trapping, separation, and transfer for $\text{S}-\text{g-C}_3\text{N}_4$ were also revealed by PL analysis (Fig. 11). The peaks of $\text{g-C}_3\text{N}_4$ and $\text{S}-\text{g-C}_3\text{N}_4$ were centered at around 450 nm, and the PL intensity of was much lower than $\text{g-C}_3\text{N}_4$, and the intensity for $\text{S}-\text{g-C}_3\text{N}_4$ decreased from $\text{S}_1-\text{g-C}_3\text{N}_4$ to $\text{S}_3-\text{g-C}_3\text{N}_4$, suggesting doping sulfur is beneficial to lowering the recombination rate of charge carriers [66].

In order to further reveal the origin of the photocatalytic activity of $\text{S}-\text{g-C}_3\text{N}_4$, we performed DFT calculations to study the electronic properties of the $\text{g-C}_3\text{N}_4$ and $\text{S}-\text{g-C}_3\text{N}_4$ and the binding interactions with U(VI) ion (Fig. 12). The energy gap between the highest occupied molecular orbital (HOMO) and the lowest unoccupied molecular orbital (LUMO) was obviously lowered from 1.51 eV (structure model of $\text{g-C}_3\text{N}_4$) to 0.81 (replacing the 2 site N with S) and 0.84 eV (replacing the 3 site N with S) (Fig. 12A). The lowered HOMO-LUMO gap favors the light energy harvesting of the photocatalysts. Moreover, the S–C bonds (1.62–1.84 Å) are generally longer than the N–C bonds (1.35 ~ 1.46 Å), which would lead to the expansion of the melem unit, and thus narrow the adsorption space

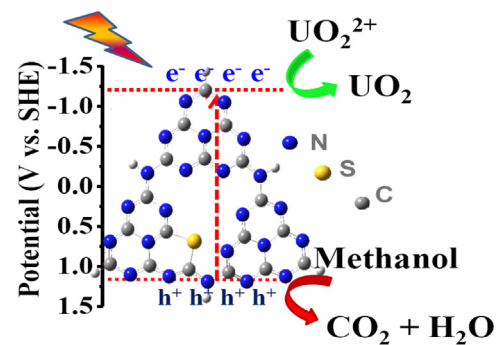


Fig. 13. The photocatalytic reduction reaction and charge transfer mechanism of the $\text{S}-\text{g-C}_3\text{N}_4$ photocatalyst under visible light irradiation.

(Fig. 12B). Therefore, the adsorption of U(VI) on the hollow site of the $\text{S}-\text{g-C}_3\text{N}_4$ (replacing N atom of two sites by S individually) would deform the structure of $\text{S}-\text{g-C}_3\text{N}_4$, and the S-substitution favors the binding of the U(VI) ions on the surface of $\text{S}-\text{g-C}_3\text{N}_4$ as reflected by the decrease of the BE from -120.13 eV for $\text{g-C}_3\text{N}_4$ to -121.00 and -121.47 eV for the two $\text{S}-\text{g-C}_3\text{N}_4$ cases.

On the basis of the above experimental and theoretical results, a possible mechanism is proposed to explain the significantly enhanced photocatalytic activity of the $\text{S}-\text{g-C}_3\text{N}_4$ photocatalyst, as shown in Fig. 13. Doping sulfur into $\text{g-C}_3\text{N}_4$ can narrow the energy gap of $\text{g-C}_3\text{N}_4$ by tuning the CB and VB levels of $\text{S}-\text{g-C}_3\text{N}_4$, and electrons were excited from the top of the band of VB to the CB of $\text{S}-\text{g-C}_3\text{N}_4$ under visible light irradiation. Owing to lowering the BE of U(VI) on the surface of $\text{S}-\text{g-C}_3\text{N}_4$, UO_2^{2+} ions can easily adsorb on the $\text{S}-\text{g-C}_3\text{N}_4$, and the photogenerated electron can be transferred to U(VI), and thus U(VI) was eventually reduced to U(IV), and the remaining hole on the VB was trapped with methanol.

4. Conclusion

We developed the photocatalytic reduction technology to remove U(VI) pollutant with sulfur doped $\text{g-C}_3\text{N}_4$ as photocatalyst

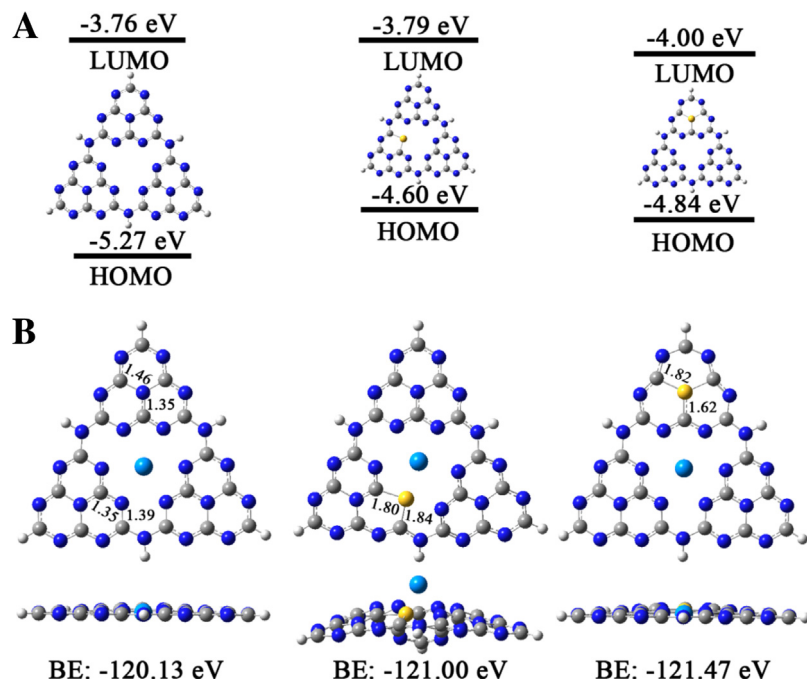


Fig. 12. (A) Molecular orbital energies and structures of the $\text{g-C}_3\text{N}_4$ and $\text{S}-\text{g-C}_3\text{N}_4$ as well as (B) the coordination complexes with U(VI) ion. Gray: C, blue: N, Yellow: S and Cyan: U(VI). (For interpretation of the references to color in this figure legend, the reader is referred to the web version of this article.)

under the visible light irradiation. The key issue of the technology is the rational design of the metal-free S-g-C₃N₄ photocatalyst with the merits of low-cost, easy scale up, and environmental friendliness. The resultant S-g-C₃N₄ shows the highly efficient photoactivity in the photocatalytic reduction of U(VI), which could be attributed to (i) the good low-band gap energy of S-g-C₃N₄ obtained by introducing sulfur into g-C₃N₄ to tune its CB and VB levels, and (ii) excellent efficiency of electron-hole separation and carrier mobility. These results strongly suggest that enhancing the reduction removal efficiency of U(VI) pollutant should be achieved by doping strategies to design potentially efficient metal-free photocatalysts (doping S, P, and other elements with suitable size and electronegativity).

Acknowledgments

This work was partially supported by the National Natural Science Foundation of China (21103019, 21307011, 21303271, and 51462002), the National Basic Research Program of China (NO. 2014CB460604), the Program of Jiangxi Provincial Department of Science and Technology (20142BAB213011), and the Foundation of Key Laboratory of Radioactive Geology and Exploration Technology Fundamental Science for National Defense (Z201408). This research is financially supported by the General Financial Grant from the China Postdoctoral Science Foundation (2014M562075 and 2015T80849).

Appendix A. Supplementary data

Supplementary data associated with this article can be found, in the online version, at <http://dx.doi.org/10.1016/j.apcatb.2016.07.036>.

References

- [1] J.Q. Niagu, J.M. Pacyna, *Nature* 333 (1988) 134–139.
- [2] S.J. Morrison, R.R. Spangler, *Environ. Sci. Technol.* 26 (1992) 1922–1931.
- [3] L.H.S. Veiga, E.C.S. Amaral, H.M. Fernandes, *J. Environ. Radioact.* 39 (1998) 69–85.
- [4] Z.J. Li, Y.Y. Yuan, Y.L. Liu, Y.L. Zhao, Z.F. Chai, W.Q. Shi, *Chem. Eng. J.* 210 (2012) 539–546.
- [5] Z.J. Li, L. Wang, L.Y. Yuan, C.L. Xiao, L. Mei, L.R. Zheng, J. Zhang, J.H. Yang, Y.L. Zhao, Z.T. Zhu, Z.F. Chai, W.Q. Shi, *J. Hazard. Mater.* 290 (2015) 26–33.
- [6] D.L. Clark, D.E. Hobart, M.P. Neu, *Chem. Rev.* 95 (1995) 25–48.
- [7] G. Choppin, *J. Radioanal. Nucl. Chem.* 273 (2007) 695–703.
- [8] S. Yan, B. Hua, Z.Y. Bao, J. Yang, C.X. Liu, B.L. Deng, *Environ. Sci. Technol.* 44 (2010) 7783–7789.
- [9] Y. Wang, M. Frutschi, E. Suvorova, V. Phrommavanh, M. Descotes, A.A.A. Osman, G. Geipel, R. Bernier-Latmani, *Nat. Commun.* 4 (2013) 2942.
- [10] D.S. Alessi, J.S. Lezama-Pacheco, J.E. Stubbs, M. Janousch, J.R. Bargar, P. Person, R. Bernier-Latmani, *Geochim. Cosmochim. Acta* 131 (2014) 115–127.
- [11] M. Dickinson, T.B. Scott, *J. Hazard. Mater.* 178 (2010) 171–179.
- [12] Y.B. Sun, C.C. Ding, W.C. Cheng, X.K. Wang, *J. Hazard. Mater.* 280 (2014) 399–408.
- [13] B. Gu, L. Liang, M.J. Dickey, X. Yin, S. Dai, *Environ. Sci. Technol.* 32 (1998) 3366–3373.
- [14] V.N. Salomone, J.M. Meichtry, G. Zampieri, M.I. Litter, *Chem. Eng. J.* 261 (2015) 27–35.
- [15] C.C. Wang, X.D. Du, J. Li, X.X. Guo, P. Wang, J. Zhang, *Appl. Catal. B: Environ.* 193 (2016) 198–216.
- [16] B.A. Marinho, R.O. Cristovao, J.M. Loureiro, R.A.R. Boaventura, V.J.P. Vilar, *Appl. Catal. B: Environ.* 192 (2016) 208–219.
- [17] Y.K. Kim, S.H. Lee, J.H. Ryu, H.W. Park, *Appl. Catal. B: Environ.* 163 (2015) 584–590.
- [18] E. Selli, V. Eliet, M.R. Spini, G. Bidoglio, *Environ. Sci. Technol.* 34 (2000) 3742–3748.
- [19] V.N. Salomone, J.M. Meichtry, G. Schinelli, A.G. Leyva, M.I. Litter, *J. Photochem. Photobiol. A: Chem.* 277 (2014) 19–26.
- [20] Q.P. Wu, J. Zhao, G.H. Qin, C.Y. Wang, X.L. Tong, S. Xue, *Appl. Catal. B: Environ.* 142–143 (2013) 142–148.
- [21] S.J. Liang, L.R. Wen, S. Lin, J.H. Bi, P.Y. Feng, X.Z. Fu, L. Wu, *Angew. Chem. Int. Ed.* 53 (2014) 2951–2955.
- [22] S.Y. Zhu, S.J. Liang, J.H. Bi, M.H. Liu, L.M. Zhou, L. Wu, X.X. Wang, *Green Chem.* 18 (2016) 1355–1363.
- [23] X.C. Wang, K. Maeda, A. Thomas, K. Takanabe, G. Xin, J.M. Carlsson, K. Domen, M. Antonietti, *Nat. Mater.* 8 (2009) 76–80.
- [24] S.W. Cao, J.X. Low, J.G. Yu, M. Jaroniec, *Adv. Mater.* 27 (2015) 2150–2176.
- [25] J.S. Zhang, X.F. Chen, K. Takanabe, K. Maeda, K. Domen, J.D. Epping, X.Z. Fu, M. Antonietti, X.C. Wang, *Angew. Chem. Int. Ed.* 49 (2010) 441–444.
- [26] L.M. Sun, X. Zhao, C.J. Jia, Y.X. Zhou, X.F. Cheng, P. Li, L. Liu, W.L. Fan, *J. Mater. Chem.* 22 (2012) 23428–23438.
- [27] X.C. Wang, S. Blechert, M. Antonietti, *ACS Catal.* 2 (2012) 1596–1606.
- [28] S.W. Cao, J.G. Yu, *J. Phys. Chem. Lett.* 5 (2014) 2101–2107.
- [29] J.S. Zhang, M.W. Zhang, G.G. Zhang, X.C. Wang, *ACS Catal.* 2 (2012) 940–948.
- [30] Q. Huang, J.G. Yu, S.W. Cao, C. Cui, B. Cheng, *Appl. Surf. Sci.* 358 (2015) 350–355.
- [31] G.G. Zhang, M.W. Zhang, X.X. Ye, X.Q. Qiu, S. Lin, X.C. Wang, *Adv. Mater.* 26 (2014) 805–809.
- [32] Y. Zheng, L.H. Lin, B. Wang, X.C. Wang, *Angew. Chem. Int. Ed.* 54 (2015) 12868–12884.
- [33] D.D. Zheng, G.G. Zhang, X.C. Wang, *Appl. Catal. B: Environ.* 179 (2015) 479–488.
- [34] Z.A. Lan, G.G. Zhang, X.C. Wang, *Appl. Catal. B: Environ.* 192 (2016) 116–125.
- [35] D.D. Zheng, C.Y. Pang, X.C. Wang, *Chem. Commun.* 51 (2015) 17467–17470.
- [36] J.S. Zhang, Y. Chen, X.C. Wang, *Energy Environ. Sci.* 8 (2015) 3092–3108.
- [37] Q.Y. Lin, L. Li, S.J. Liang, M.H. Liu, J.H. Bi, L. Wu, *Appl. Catal. B: Environ.* 163 (2015) 135–142.
- [38] S.J. Liang, Y.Z. Xia, S.Y. Zhu, S. Zheng, Y.H. He, J.H. Bi, M.H. Liu, L. Wu, *Appl. Surf. Sci.* 358 (2015) 304–312.
- [39] F.F. Liang, Y.F. Zhu, *Appl. Catal. B: Environ.* 180 (2016) 324–329.
- [40] M. Zhang, W.J. Luo, Z. Wei, W.J. Jiang, D. Liu, Y.F. Zhu, *Appl. Catal. B: Environ.* 194 (2016) 105–110.
- [41] G. Liu, P. Niu, C.H. Sun, S.C. Smith, Z.G. Chen, G.Q. Lu, H.M. Cheng, *J. Am. Chem. Soc.* 132 (2010) 11642–11648.
- [42] L.L. Feng, Y. Zou, C. Li, S. Gao, L.J. Zhou, *Int. J. Hydrogen Energy* 39 (2014) 15373–15379.
- [43] L. Cao, R. Wang, D.X. Wang, *Mater. Lett.* 149 (2015) 50–53.
- [44] J.L. Chen, Z.H. Hong, Y.L. Chen, B.Z. Lin, B.F. Gao, *Mater. Lett.* 145 (2015) 129–132.
- [45] H.B. Tao, H.B. Yang, J.Z. Chen, J.W. Miao, B. Liu, *Beilstein J. Nanotechnol.* 3 (2014) 770–777.
- [46] J.N. Zhao, L. Ma, H.Y. Wang, Y.F. Zhao, J. Zhang, S.Z. Hu, *Appl. Surf. Sci.* 332 (2015) 625–630.
- [47] H.Q. Ma, Y. Li, S. Li, N. Liu, *Appl. Surf. Sci.* 357 (2015) 131–138.
- [48] Z.Z. Lin, X.C. Wang, *Angew. Chem. Int. Ed.* 52 (2013) 1735–1738.
- [49] K. Wang, Q. Li, B.S. Liu, B. Cheng, W.K. Ho, J.G. Yu, *Appl. Catal. B: Environ.* 176 (2015) 44–52.
- [50] Y.J. Zhang, T. Mori, J.H. Ye, M. Antonietti, *J. Am. Chem. Soc.* 132 (2010) 6294–6295.
- [51] G.D. Ding, W.T. Wang, T. Jiang, B.X. Han, H.L. Fan, G.Y. Yang, *ChemCatChem* 5 (2013) 192–200.
- [52] M. Zhang, X.J. Bai, D. Liu, J. Wang, Y.F. Zhu, *Appl. Catal. B: Environ.* 164 (2015) 77–81.
- [53] X.G. Ma, Y.H. Lv, J. Xu, Y.F. Liu, R.Q. Zhang, Y.F. Zhu, *J. Phys. Chem. C* 116 (2012) 23485–23493.
- [54] J.G. Yu, K. Wang, W. Xiao, B. Cheng, *Phys. Chem. Chem. Phys.* 16 (2014) 11492–11501.
- [55] Z.L. Ma, S. Dou, A.L. Shen, L. Tao, L.M. Dai, S.Y. Wang, *Angew. Chem. Int. Ed.* 54 (2015) 1888–1892.
- [56] J.S. Zhang, J.H. Sun, K. Maeda, K. Domen, P. Liu, M. Antonietti, X.Z. Fu, X.C. Wang, *Energy Environ. Sci.* 4 (2011) 675–678.
- [57] J.D. Hong, X.Y. Xia, Y.S. Wang, R. Xu, *J. Mater. Chem.* 22 (2012) 15006–15012.
- [58] D.D. Shao, Z.Q. Jiang, X.K. Wang, J.X. Li, Y.D. Meng, *J. Phys. Chem. B* 113 (2009) 860–864.
- [59] Y.B. Sun, S.B. Yang, Y. Chen, C.C. Ding, W.C. Cheng, X.K. Wang, *Environ. Sci. Technol.* 49 (2015) 4255–4262.
- [60] C.H. Lu, R.Y. Chen, X. Wu, M.F. Fan, Y.H. Liu, Z.G. Le, S.J. Jiang, S.Q. Song, *Appl. Surf. Sci.* 360 (2016) 1016–1022.
- [61] L. Wang, X.Y. Li, W. Teng, Q.D. Zhao, Y. Shi, R.L. Yue, Y.F. Chen, *J. Hazard. Mater.* 244–245 (2013) 681–688.
- [62] X.J. Liu, L.K. Pan, T. Lv, G. Zhu, Z. Sun, C.Q. Sun, *Chem. Commun.* 47 (2011) 11984–11986.
- [63] Y.C. Zhang, J. Li, M. Zhang, D.D. Dionysiou, *Environ. Sci. Technol.* 45 (2011) 9324–9331.
- [64] X.F. Wang, S.F. Li, H.G. Yu, J.G. Yu, *J. Mol. Catal. A: Chem.* 334 (2011) 52–59.
- [65] J.Y. Zhang, Y.H. Wang, J. Zhang, Z. Lin, F. Huang, J.G. Yu, *ACS Appl. Mater. Interfaces* 5 (2013) 1031–1037.
- [66] M. Xu, L. Han, S.J. Dong, *ACS Appl. Mater. Interfaces* 5 (2013) 12533–12540.